

University of Oklahoma Advanced Radar Research Center PX-1000 Data Plains Elevated Convection At Night (PECAN) Experiment

Contacts/PIs:

Boon Leng Cheong
boonleng@ou.edu

James Kurdzo
kurdzo@ou.edu

David Bodine
dbodine@ucar.edu

Mailing address:
Boon Leng Cheong
Advanced Radar Research Center
3190 Monitor Avenue
Norman, OK 73019

Please contact us with any questions or comments on the dataset, or about collaboration opportunities.

1. PX-1000 Dataset Overview

During the Plains Elevated Convection At Night (PECAN) experiment, the University of Oklahoma (OU) Advanced Radar Research Center's (ARRC) PX-1000 radar was deployed as part of the mobile radar hexagon in support of MCS, LLJ, bore, and pristine CI missions. PX-1000 was primarily utilized in MCS and CI missions due to its relatively low sensitivity, but did take part in occasional LLJ and bore missions. PX-1000 was often placed on the western edge of the radar hexagon by the Radar Coordinator, and therefore was often the first radar to be impacted by severe or near-severe wind gusts. A brief overview of the PX-1000 platform can be accessed at <https://arrc.ou.edu/px1000.html>.

This dataset includes data beginning on 22 June 2015 and ending on 14 July 2015. The primary scanning mode was volumetric; however multiple scanning strategies were used based on requests of the Radar Coordinator. A number of RHI scans were completed in support of the NCAR/EOL Parsivel disdrometer mission (contact: David Bodine, dbodine@ucar.edu) and the NASA/JPL DC-8 mission (contact: Simone Tanelli, simone.tanelli@jpl.nasa.gov).

2. PX-1000 Instrument Description and Data Processing

The PX-1000 radar is a transportable, polarimetric, X-band, dish-based platform mounted on a trailer that can be moved as necessary for various field campaign requirements (Table 1; Cheong et al. 2013a). Operating at 200-W peak power on each channel (for

simultaneous independent H/V transmit/receive), the pulse compression scheme described in Kurdzo et al. (2014) is used in order to achieve the necessary sensitivity for meteorological data collection. The resulting sensitivity is approximately 14dBZ at 50-km range, and the native range resolution is 112 m. The 1.8-m-diameter parabolic dish results in a 1.88-deg azimuthal resolution at 9.55 GHz. The range gates and azimuths are oversampled to 30 m and 1 deg, respectively.

Because of the use of pulse compression, a blind range during transmission of the long pulse (67 μ s) exists, meaning no returns can be measured within 10.3 km of the radar. To mitigate this issue, the time-frequency multiplexing (TFM) method described in Cheong et al. (2013a) is utilized to fill the blind range with a short pulse (2 μ s). The resulting sensitivity is lower in the 10.3 km surrounding the radar (Fig. 1), however, strong echoes such as those associated with convection are sufficiently resolved and do not hinder the analysis presented in this dataset. This discrepancy is more apparent in weaker echoes, as seen in Fig. 2 where a circular area of lower sensitivity is apparent.

Additionally, in order to achieve high-quality estimates, the multilag method detailed in Lei et al. (2012) is used for moment estimation. The multilag method is especially valuable for ρ_{HV} estimation in low signal-to-noise ratio (SNR) situations. This method, when combined with the TFM technique, allows for ρ_{HV} estimates that are less susceptible to low SNRs, resulting in significantly increased accuracy and smooth transitions across the blind range (Cheong et al. 2013b). It is important to note that in areas of high spectrum width, the multilag Gaussian fit does not hold and the multilag assumption will not hold (Kurdzo et al. 2015). PX-1000 I/Q data were processed with a TFM matched filter to generate moment data. A total of 100 pulses were used for moment estimates.

Table 1: PX-1000 system characteristics

PX-1000 System Characteristics	
Transmitter Type	Dual Solid-State Power Amplifiers
Operating Frequency	9550 MHz
PRF	1-2000 Hz
Radiating Center	2.5 m AGL
Sensitivity	<17 dBZ at 50 km
Observable Range	60 km
Antenna Gain	38.5 dBi
Antenna Diameter	1.8 m
3-dB Beamwidth	1.8 deg
Polarization	Dual linear, simultaneous H/V (SHV)
Polarimetric Isolation	26 dB
Max Rotation Rate	50 deg/s
Peak Power	200 W
Pulse Width	1-69 μ s
Chirp Bandwidth	5 MHz
Maximum Duty Cycle	20%
Minimum Gate Spacing	30 m

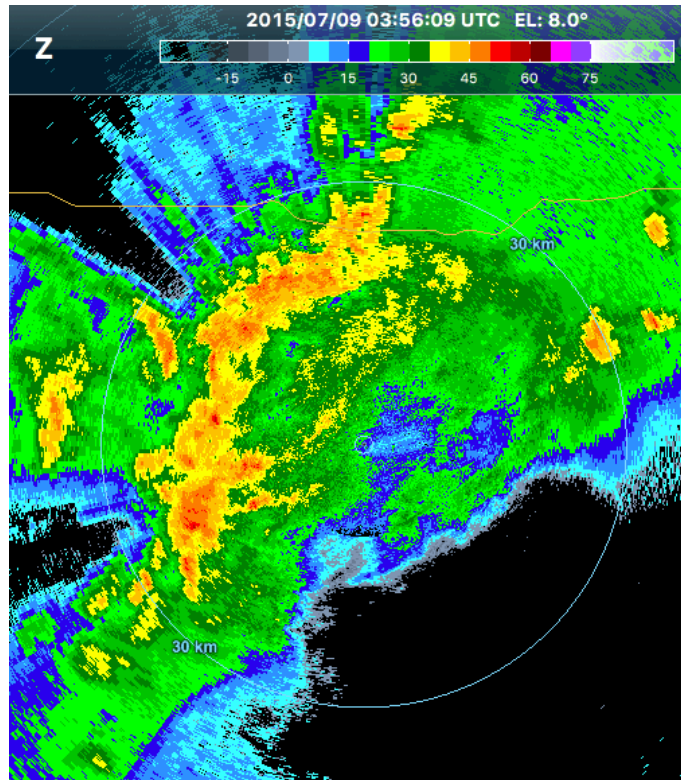


Fig. 1: Reflectivity factor data masking the blind range (strong echoes).

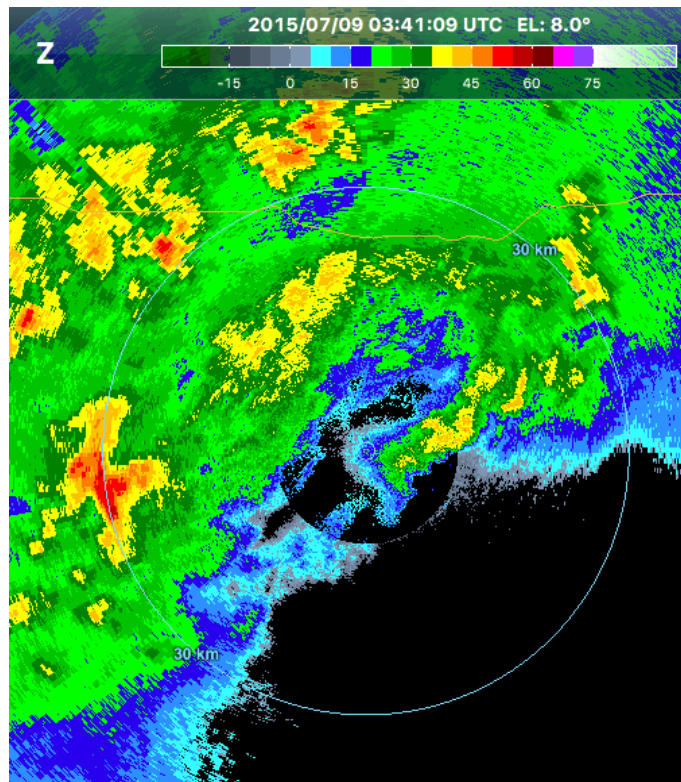


Fig. 2: Reflectivity factor data revealing the blind range (weak echoes).

3. Data Format

The dataset has been converted from an in-house netCDF format to CFradial files using a converter written for the PECAN project. Each volume in a deployment is labeled starting at volume 1, with each elevation being labeled as a different sweep, starting at sweep 1. These values are consistently marked in the file naming scheme. For example:

```
cfrad.20150709_021812_PX1000_v7_s10.nc
```

This file indicates CFradial format, a date of 09 July 2015, a time of 0218:12 UTC, from the PX-1000 radar, volume number 7, and sweep number 10.

RHIs are grouped into the previous volume if there are two or fewer RHIs after a volume. If there are more than two RHIs, they are grouped as their own volume. For example, adding an RHI at the end of 12 sweeps will end up in an RHI being recorded as sweep 13. However, if 6 RHIs are complete back-to-back, they will all fall under a single volume with 6 different sweeps.

Parameters included in most deployments are:

Z – Horizontal Reflectivity Factor (dBZ)

V – Radial Velocity (m/s)

W – Spectrum Width (m/s)

Z_{DR} – Differential Reflectivity (dB)

ρ_{HV} – Correlation Coefficient (unitless)

ϕ_{DP} – Differential Phase (deg)

4. Data Remarks

Data for PECAN with PX-1000 only includes the timeframe between 22 June 2015 and 14 July 2015. Due to split deployments near the end of the project, PX-1000 was not on all relevant missions. PX-1000 did not participate in PECAN operations on 15 July 2015.

Due to the use of a low-power solid-state transmitter, the sensitivity issues within and around the blind range can manifest themselves in different ways. The figures in this section demonstrate examples of potential issues.

(a) Waveforms and Pulse Lengths

The primary waveform for PX-1000 has three main goals: high sensitivity, long range, and low sidelobes. This is possible through the use of the maximum pulse length (for sensitivity and range) and the optimization procedure from Kurdzo et al. 2014 to minimize sidelobes while limiting windowing. The primary waveform provides excellent performance out to roughly 60 km, but at one major cost: the blind range. This is mitigated with the fill pulse, but even out to only 10.3 km, a 2 μ s pulse is not sufficiently sensitive at

200 W peak power. This means that if the feature of interest has low reflectivity and is close to the radar, the region inside the blind range can suffer enough in sensitivity to make the radar unusable for the desired mission.

Clear air phenomena are wide and varied, but two specific cases will be investigated in this section: gust front passages and clear air wind observations. Both of these cases involve the necessity to shorten the blind range as much as possible while still achieving significant sensitivity increases from pulse compression. Of course, a short pulse length results in lower overall sensitivity, but it increases the sensitivity in the original blind range and shortens the range necessary for a fill pulse. With the dependence on r^2 in the radar equation, ranges very close to the radar do not need as long of a pulse length to achieve high sensitivity; this is the same principle that the fill pulse operates on, but it is shortened here to observe weak targets within the original blind range.

For the examples presented in this section, a target pulse length was roughly 5 μ s, or 33.5 μ s (half the original pulse length of PX-1000). Using the same 2.2 MHz of bandwidth for the long pulse, this results in a TB product of 73.7. However, since the absolute maximum sensitivity is desired, *absolutely no windowing* was applied to this design. The resulting matched filter response, then, displays very high sidelobes. With a peak sidelobe level of -44 dB in theory, and worse in practice, these sidelobes are not ideal for a weather radar. However, it is important to realize that the phenomena being observed are *low-reflectivity* targets, meaning they are likely to be just above the noise floor. This means that any sidelobes below 20-25 dB are likely to be sufficient for these examples. In addition, the transmitters were driven entirely into saturation with this waveform, causing higher distortion rates but gaining 1-2 dB of additional sensitivity. This would not normally be done if sidelobes were a concern with little windowing.

As part of PECAN, there were four main mission goals: observations of MCSs, bores, pristine CI, and the LLJ. MCSs and bores generally involve one or more "fine lines" of outflow or oscillatory waves. These phenomena typically pick up small amounts of insects, bugs, and dirt, lofting them into the radar beam at the head of a density current. A high-powered radar can receive enough scattered energy off of these relatively low densities of targets due to their size. Part of the PECAN mission goal was to observe the dynamics of these outflow boundaries and bores and how new convection initiates off of them. Since density currents associated with outflow are generally low-level phenomena, they are best observed within 10-15 km of a radar. An example from PECAN of an outflow boundary ahead of a bowing MCS that later became a bore is shown in Fig. 3 just before encountering the blind range.

Unfortunately, with a 10.3-km blind range and a short fill pulse, this often leads to a ring of sensitivity that is too low to observe outflow boundaries between approximately 5-10 km. This is shown in Fig. 4, where the outflow boundary is crossing through the 5-10 km range within the fill pulse. The short pulse is not able to see the outflow boundary, causing a significant discontinuity.

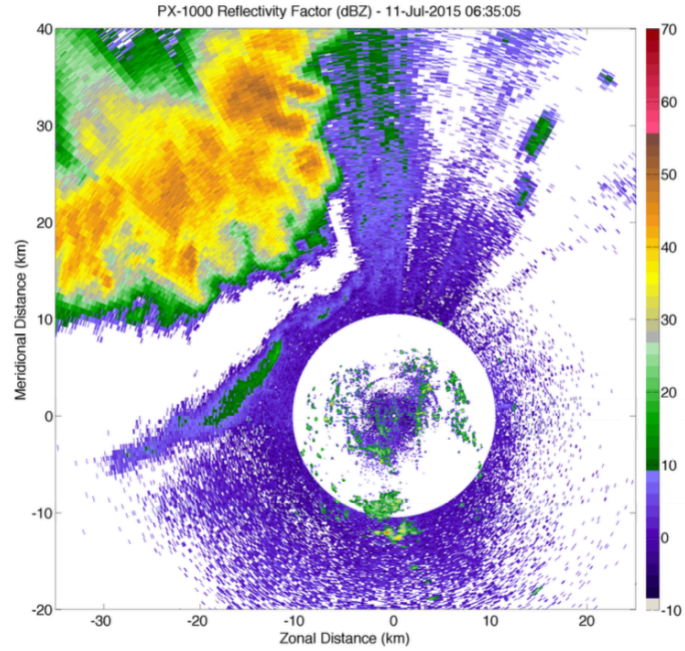


Fig. 3: Reflectivity factor showing an outflow boundary ahead of an MCS approaching the blind range.

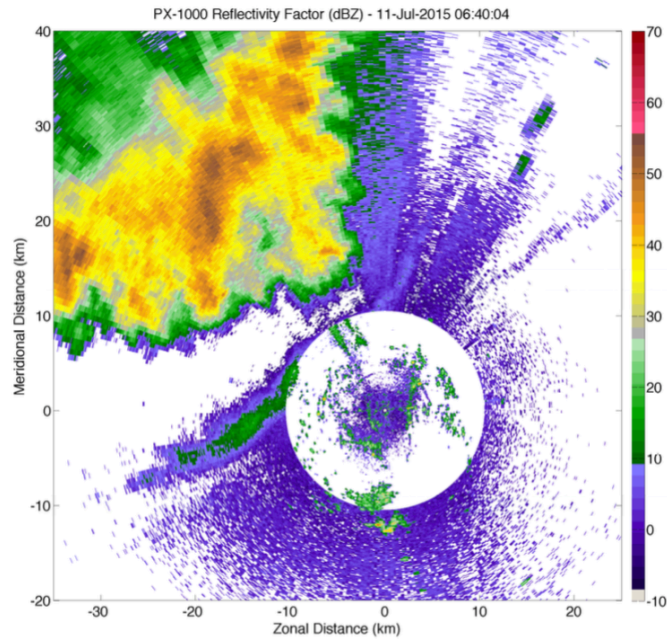


Fig. 4: Reflectivity factor showing an outflow boundary ahead of an MCS partially inside the blind range. The outflow boundary can not be resolved, even with the fill pulse due to its low reflectivity and the short pulse length.

Since the focus of this case is the outflow boundary, sidelobes are not a critical issue due to its low reflectivity. Therefore, in Fig. 5, PX-1000 was switched to the 5 km pulse. The outflow boundary was crossing into the 5-km range, but a significant proportion was still in the 5-10 km range. The entirety of the boundary was observable in this mode, essentially culling the issue seen in Fig. 4. There are some radial spikes of energy apparent near the radar from clutter sidelobes, but this is largely due a limitation of the existing ground clutter filter and the blind range transition.

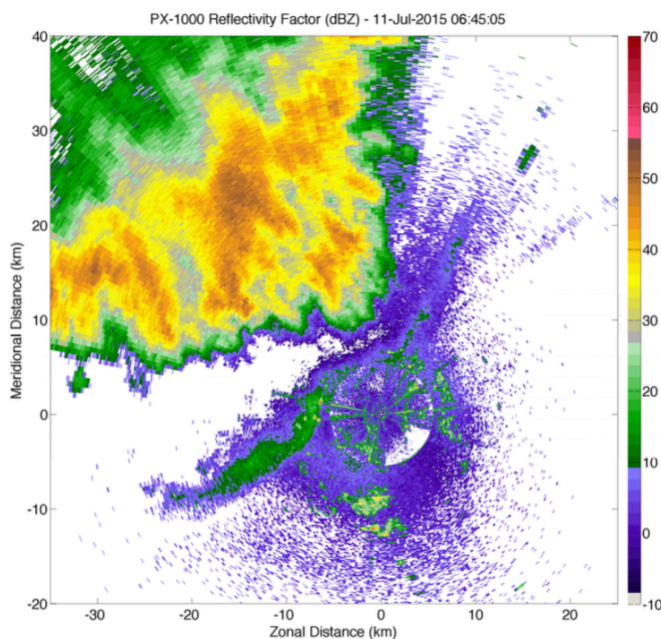


Fig. 5: Reflectivity factor showing an outflow boundary ahead of an MCS inside the original blind range (10.3 km) and crossing into the new blind range (with a 5 km pulse). The vast majority of the outflow boundary is observable, especially in the 5-10 km ranges.

An additional mission of PECAN was observation of the LLJ. The LLJ is a strengthening of the horizontal wind field at the top of the decoupled nocturnal boundary layer that is often responsible for isentropic lift over frontal boundaries resulting in thunderstorm development at night. The LLJ was observed by in-situ methods (radiosondes and tethered balloons) and remote methods (lidar, sodar, and radar). The technique used for radar observations of the LLJ is called a velocity azimuth display (VAD) wind profile (VWP), which provides horizontal wind estimates using a volumetric scanning strategy. A VWP utilizes the fact that different range gates are associated with different heights. As the radar rotates, the radial wind direction and velocity creates a sine wave with the phase indicating the direction and the amplitude relating to the velocity. As the radar scans in elevation, higher heights can be recorded, similar to a Skew-T Log-P diagram used in radiosonde soundings.

In clear air modes, especially during LLJ missions as part of the PECAN project, the primary scattering mechanism was insects trapped in the boundary layer transition zone. With very low densities but large sizes, the reflectivity factor of these insects was in the

5-10 dBZ range. This was an acceptable level of sensitivity out to approximately 5 km and beyond the edge of the fill pulse, but the range between 5-10 km was left with only the short fill pulse and not enough sensitivity to get any returns above the noise floor. An example of the result is shown in Fig. 6. Note the large gap in radial velocity returns, preventing a continuous VWP in range and height. The echo to the west-northwest of the radar is a second trip return from a distant thunderstorm.

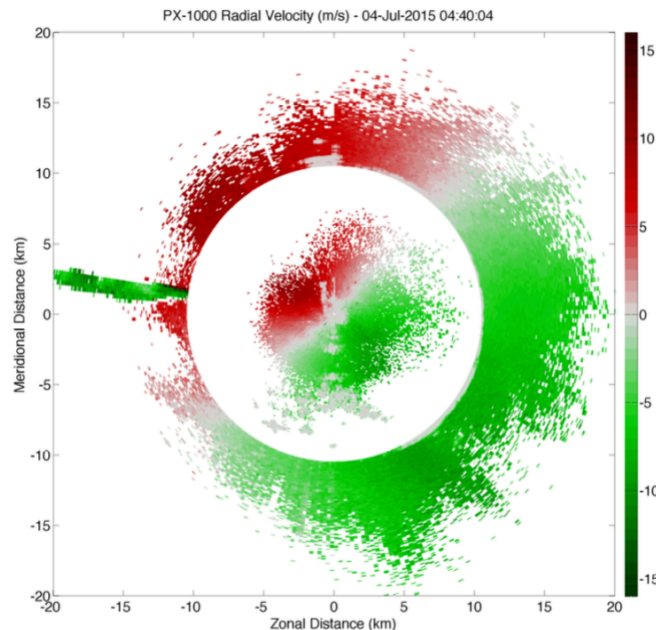


Fig 6: Radial velocity during a LLJ mission using a 10.3-km pulse. The low sensitivity from 5-10 km is due to the use of a short fill pulse not capable of seeing insects at the ranges in the original blind range, making it impossible to form consistent VWPs in range and height. Note that the echo to the WNW of the radar is a second-trip return.

Using the 5-km pulse described previously, a substantially improved picture of the wind field can be seen in Fig. 7. By using a 5-km pulse, the fill pulse only needs to be used out to 5 km, which is an acceptable range for scattering off insects with a short pulse. There remains a small ring of low sensitivity which could have been solved with a slightly shorter pulse, but such a pulse was not readily available during PECAN. The scan in Fig. 7 was approximately 10 min after Fig. 6. Using this method, consistent scans of the LLJ in range, height, and time were possible throughout the duration of PECAN.

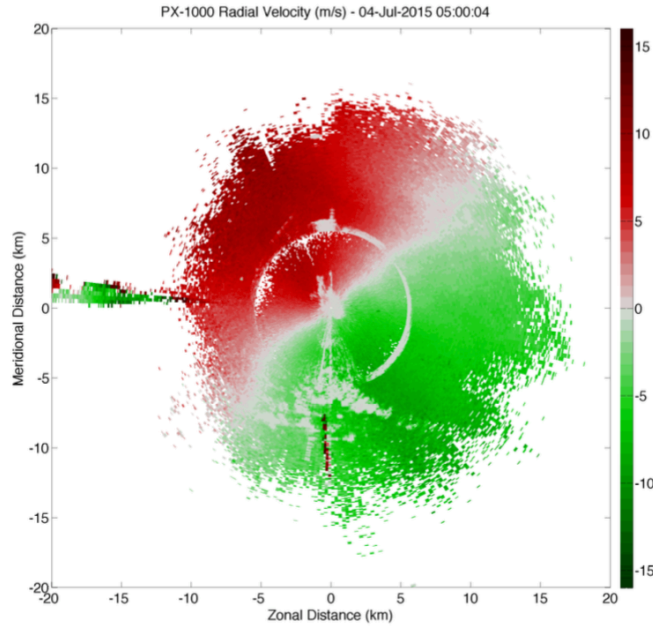


Fig. 7: Radial velocity during a LLJ mission using a 5-km pulse. The area of low sensitivity seen in Fig. 6 is mitigated by the use of a short pulse (and hence shorter blind range). Note that the echo to the WNW of the radar is a second-trip return.

(b) Wet Radome Contamination

During cases with a wet radome, typically after the passage of a convective system, contamination became evident at the edge of the blind range. These data are not real echoes and should not be used. An example is shown in Fig. 8.

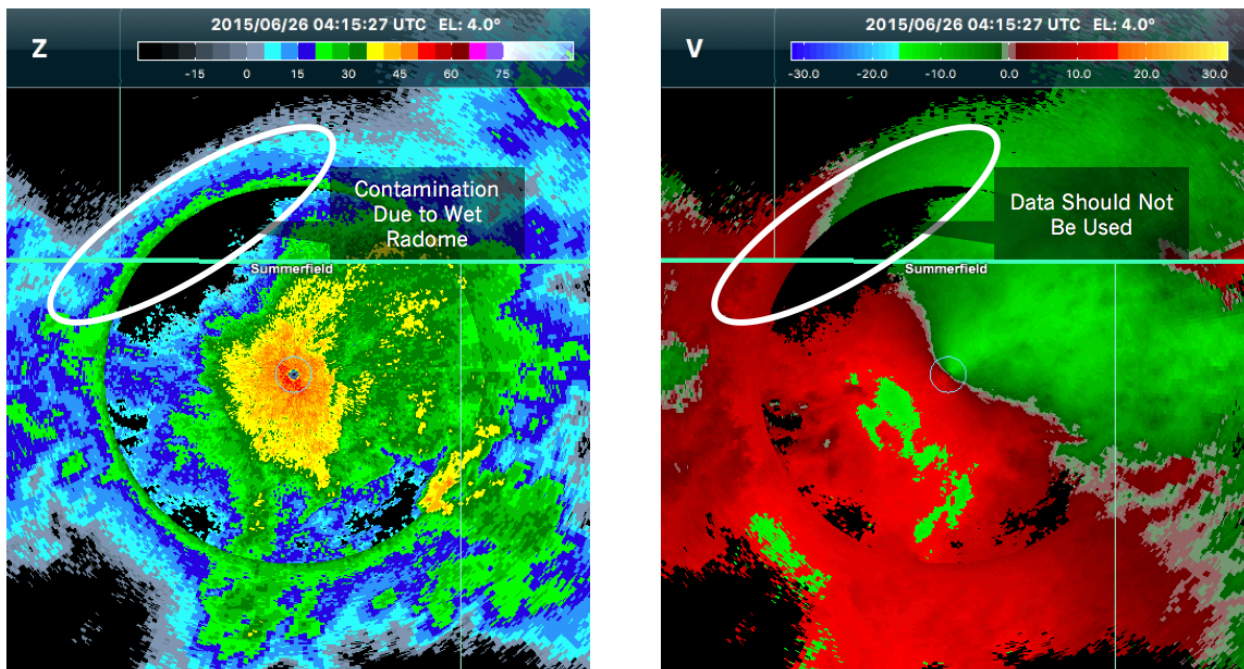


Fig. 8: Example of wet radome contamination

(c) *Waveform Leakage*

In addition to having to deal with second-trip returns, the use of a fill pulse introduces difficulty in separating second-trips between the long waveform and the fill waveform. On occasion, the far range can be folded into only the short pulse region (inside the blind range) and be masked just outside the blind range due to the higher sensitivity of the long pulse at that point in the next pulse sequence. Examples in various moment fields are shown in in Figs. 9-14.

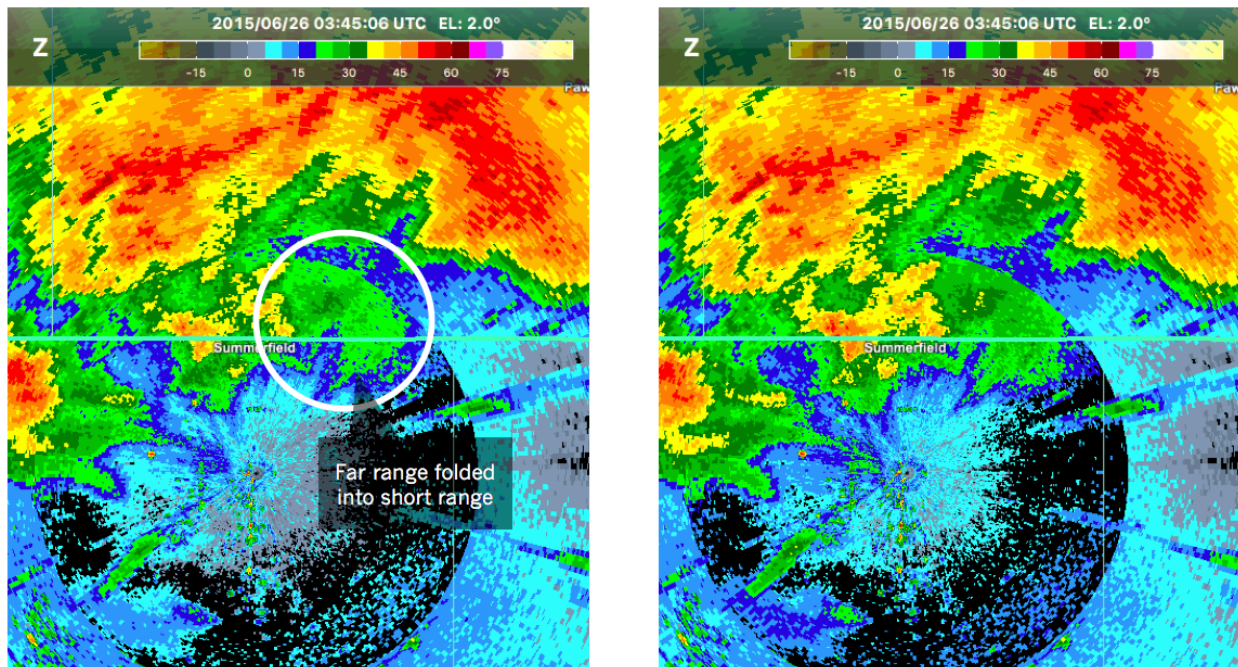


Fig. 9: Example of waveform leakage in Z.

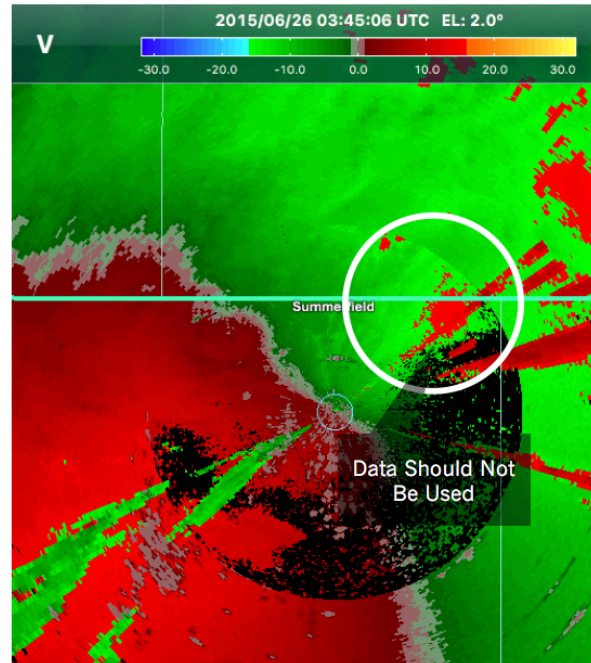
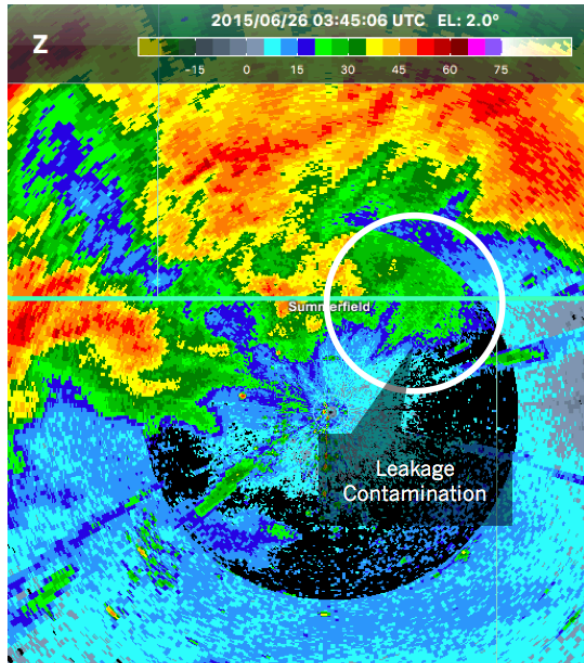


Fig. 10: Example of waveform leakage in V.

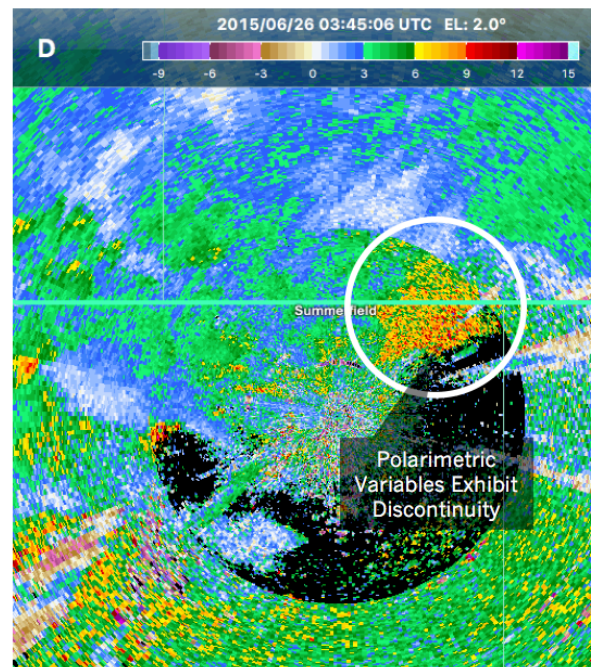
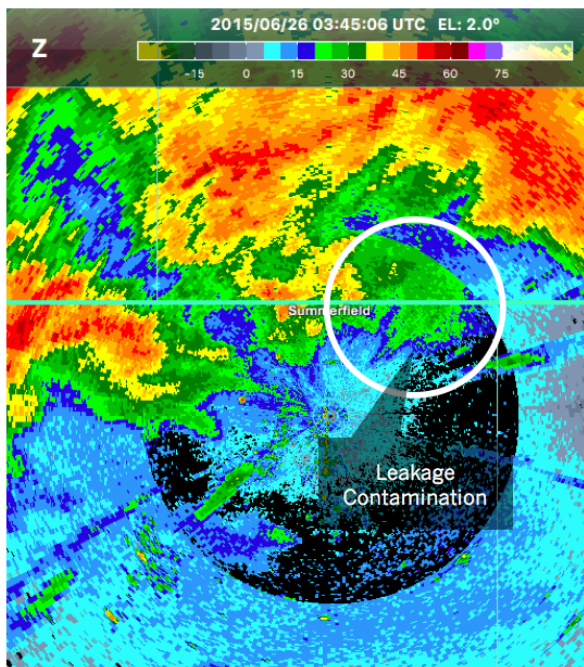


Fig. 11: Example of waveform leakage in Z_{DR} .

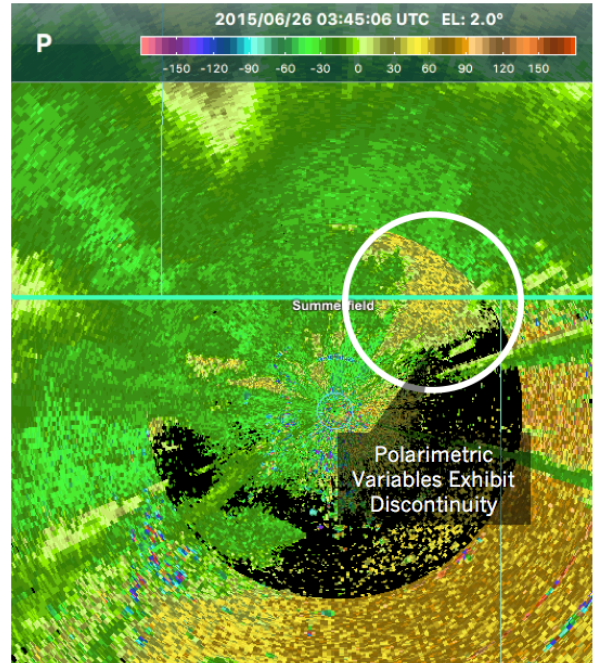
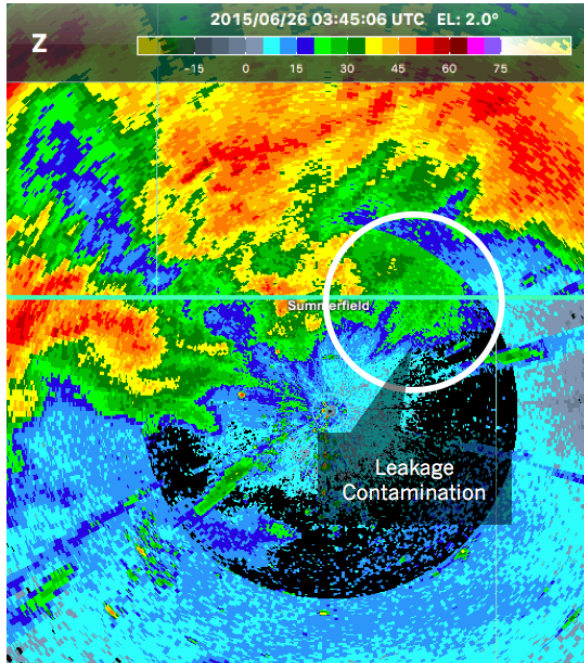


Fig. 12: Example of waveform leakage in ϕ_{DP} .

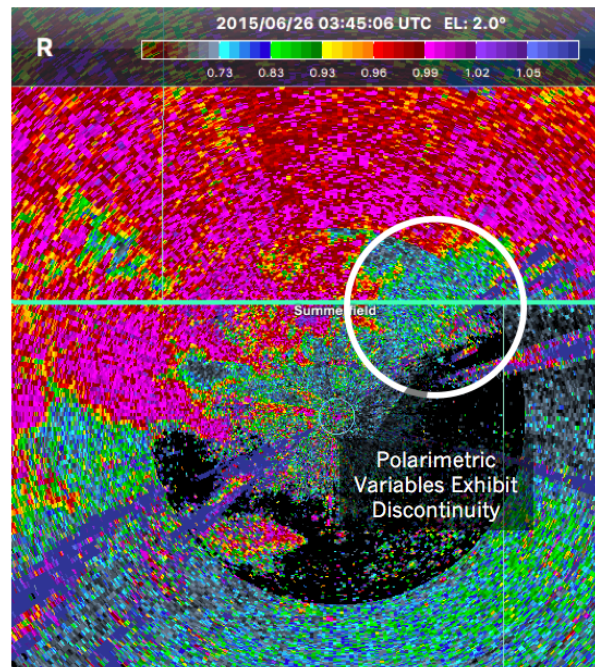
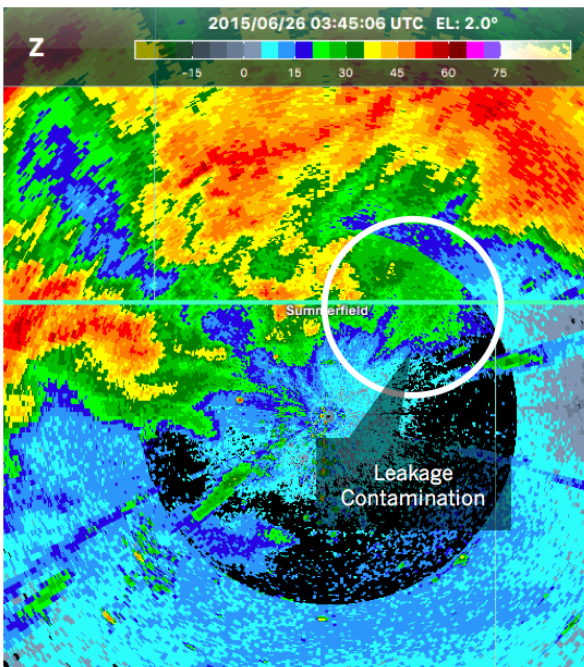


Fig. 13: Example of waveform leakage in ρ_{HV} .

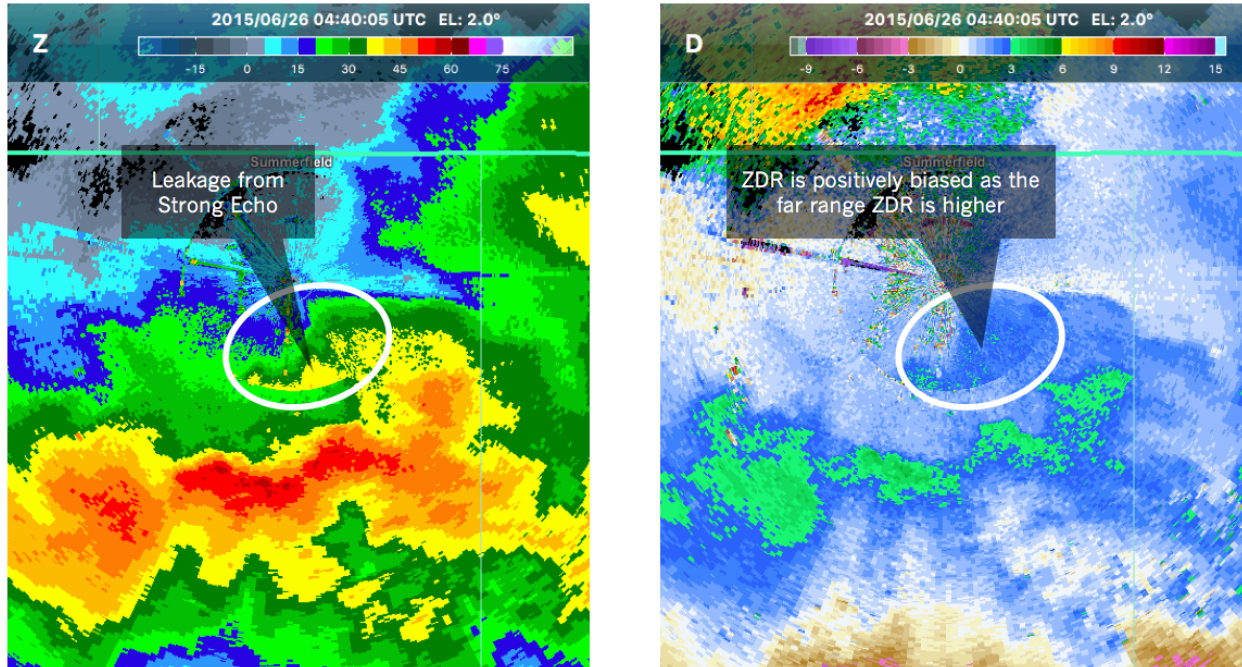


Fig. 14: Example of waveform leakage in Z_{DR} .

(d) ρ_{HV} Data on 9 July 2015

Due to an irreversible error, all ρ_{HV} data from the 9 July 2015 mission were removed from the dataset. All other moments are available in regular CFradial format.

5. References

Cheong, B. L., R. Kelley, R. D. Palmer, Y. Zhang, M. Yeary, and T.-Y. Yu, 2013a: PX-1000: A solid-state polarimetric X-band weather radar and time-frequency multiplexed waveform for blind range mitigation. *IEEE Trans. Instrum. Measure.*, 62, 3064–3072.

<http://ieeexplore.ieee.org/xpls/icp.jsp?arnumber=6558769>

Cheong, B. L., J. M. Kurdzo, G. Zhang, and R. D. Palmer, 2013b: The impacts of multi-lag moment processor on a solid-state polarimetric weather radar. *36th Conf. on Radar Meteorology*, Breckenridge, CO, Amer. Meteor. Soc., 2B.2.

<https://ams.confex.com/ams/36Radar/webprogram/Paper228464.html>

Kurdzo, J. M., B. L. Cheong, R. D. Palmer, G. Zhang, and J. Meier, 2014: A pulse compression waveform for improved-sensitivity weather radar observations. *J. Atmos. Oceanic Technol.*, 31, 2713–2731.

<http://journals.ametsoc.org/doi/abs/10.1175/JTECH-D-13-00021.1>

Kurdzo, J. M., D. J. Bodine, B. L. Cheong, and Robert D. Palmer, 2015: High-Temporal Resolution Polarimetric X-Band Doppler Radar Observations of the 20 May 2013 Moore, Oklahoma, Tornado. *Mon. Wea. Rev.*, **143**, 2711–2735.

<http://journals.ametsoc.org/doi/abs/10.1175/MWR-D-14-00357.1>

Lei, L., G. Zhang, R. J. Doviak, R. Palmer, B. L. Cheong, M. Xue, Q. Cao, and Y. Li, 2012: Multilag correlation estimators for polarimetric radar measurements in the presence of noise. *J. Atmos. Oceanic Technol.*, 29, 772–795.

<http://journals.ametsoc.org/doi/abs/10.1175/JTECH-D-11-00010.1>